Chapter 2
Remote Sensing of Drivers of Spring Snowmelt Flooding in the North Central U.S.

Samuel E. Tuttle, Eunsang Cho, Pedro J. Restrepo, Xinhua Jia, Carrie M. Vuyovich, Michael H. Cosh, and Jennifer M. Jacobs

2.1 Introduction

Melting of accumulated snow contributes significantly to runoff in northern North America and mountainous areas (up to 50–95 %) (WMO 2009). In many regions, snowmelt associated with the spring thaw creates an annual risk of flooding, which can endanger lives and damage private property and infrastructure. For instance, rapid snowpack melting and rainfall in the northeast U.S. in January 1996 led to 30 fatalities and over $1.5 billion in damages (Anderson and Larson 1996). Snowmelt flooding along the Red River of the North in 1997 damaged 85 % of all structures in Grand Forks, North Dakota, and caused a total of $4 billion in damages in the U.S. (Todhunter 2001). Weeks later, flood waters nearly overtopped levees in

S.E. Tuttle, M.A., Ph.D. (✉) • E. Cho, M.S. • J.M. Jacobs, Ph.D.
Department of Civil and Environmental Engineering, University of New Hampshire, Gregg Hall, 35 Colovos Road, Durham, NH 03824, USA
e-mail: samuel.tuttle@unh.edu; ec1072@wildcats.unh.edu; Jennifer.jacobs@unh.edu

P.J. Restrepo, Ph.D., M.Sc., Ingeniero Civil
Consulting Engineer, Minneapolis, MN, USA
e-mail: pr.engconsult@gmail.com

X. Jia, Ph.D.
Department of Agricultural and Biosystems Engineering, North Dakota State University, NDSU Dept 7620, PO Box 6050, Fargo, ND 58108, USA
e-mail: Xinhua.jia@ndsu.edu

C.M. Vuyovich, M.S.
Remote Sensing, GIS and Water Resources Branch, USACE Cold Regions Research and Engineering Laboratory, 72 Lyme Road, Hanover, NH 03755, USA
e-mail: carrie.m.vuyovich@usace.army.mil

M.H. Cosh, Ph.D.
USDA Agricultural Research Service, 10300 Baltimore Ave, Beltsville, MD 21032, USA
e-mail: Michael.Cosh@ars.usda.gov

V. Lakshmi (ed.), *Remote Sensing of Hydrological Extremes*, Springer Remote Sensing/Photogrammetry, DOI 10.1007/978-3-319-43744-6_2

Winnipeg, Manitoba, Canada, but still prompted $500–750 million in expenditures, including construction of a levee that is one of the largest peacetime efforts in Canadian history (Rannie 2016). In 2011, spring snowmelt in the north central U.S. partially contributed to major flooding in the Missouri, Souris, Ohio, and Mississippi river basins, responsible for up to $3.8 billion in direct damages (NWS-HIC 2011). Accurate river flow forecasting allows communities and governments to better plan for such flooding emergencies and mitigate the impacts of damaging floods.

Snowmelt flooding occurs when the primary source of floodwater is melting snow. Accumulated snowpack on the ground surface stores precipitated water that can be released days, weeks, or months later upon melting. Larger snowpacks store greater amounts of frozen water and have a larger risk and magnitude of spring floods. Soil moisture and soil frost status determine how much snowmelt can infiltrate into soils, because wetter soils and deeper frost (especially paired with high soil moisture) reduce infiltration, leading to more runoff (Todhunter 2001). Soil moisture status is often carried over from the late fall due to soil freezing, while the degree of soil freezing depends on winter air temperatures and the presence and depth of snow, which insulates the soil (Shanley and Chalmers 1999).

Other factors can exacerbate spring flooding. Precipitation during the spring melt adds water to the already elevated basin water content. Rainfall can increase the rate of snow melt by adding heat energy (Harr 1981). Rapid spring thaws deliver meltwater in shorter time windows and thus result in greater streamflow magnitudes (Todhunter 2001). Ice jams in river channels can impede river flows, raising the river height upstream of the blockages (Beltaos 2008). Additionally, changes in river grade may cause backwater effects (such as just north of Grand Forks, ND; Todhunter 2001), increasing flood heights. Finally, the spatial pattern of melting snow can interact with the river network configuration to deliver meltwater from individual tributaries simultaneously (increasing instantaneous flow volumes) or asynchronously (Miller and Frink 1984).

Accurate prediction of river flows due to snowmelt flooding requires knowledge of these factors, both temporally and spatially, and the ability to synthesize their interactions. However, many of these state variables, such as snow water equivalent, soil moisture, soil frost, and melt phase, are poorly spatially constrained. Traditionally, observations of these variables are provided by ground stations. However, ground stations provide only "point" observations from individual locations, and far too few stations exist in most regions to obtain a reliable spatial understanding of these hydrological states.

Fortunately, remote sensing can estimate many important drivers of snowmelt floods, including snow water equivalent (SWE) and soil moisture (among others). While many methods exist, passive microwave remote sensing has a robust history for snow and soil moisture, and thus is best prepared for operational use in flood forecasting. Significant snowmelt floods have occurred in the northern Plains of the United States. This area is well suited for passive microwave remote sensing (Vuyovich et al. 2014), so the potential for enhancing flood forecasting using remote sensing observations is high in this region.

In this chapter, we review the use of remote sensing observations to constrain snow water equivalent and soil moisture (two primary drivers of spring snowmelt floods), using the north central United States as a case study. We provide examples from previous studies where these methods have shown value, as well as specific examples from the Red River of the North basin. Attention is given to the potential for passive microwave instruments to contribute to operational flood forecasting.

2.2 Background on the Red River of the North Basin

The Red River of the North basin (RRB) provides an excellent location to showcase the challenges from snowmelt flooding in nonmountainous regions, as well as opportunities for remote sensing to contribute to scientific advancement and reduce the loss of human life and property. The Red River marks the border between the states of North Dakota and Minnesota and drains parts of eastern North Dakota, western Minnesota, and a small area of northeastern South Dakota (see Figs. 2.1 and 2.2). The river flows north from its headwaters in Wahpeton, ND to the United States–Canada border, and then on through Winnipeg, Manitoba, where it is joined by the Assiniboine River, and finally into Lake Winnipeg. In its entirety, the Red

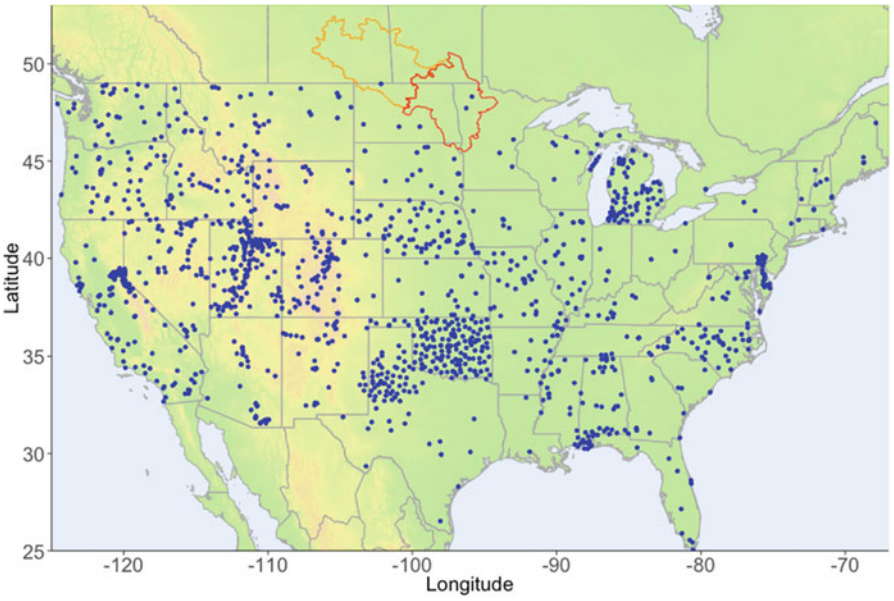

Fig. 2.1 Location of the Red River of the North basin (*red*) and observation sites that have contributed to the North American Soil Moisture Database (NASMD; *blue dots*) (Quiring et al. in press). The *red* polygon is the area of the RRB that we focus on in this chapter, and the *orange* polygon shows the tributary Assiniboine River basin. Notice the relative lack of observations available in the northern Great Plains, despite its agricultural importance

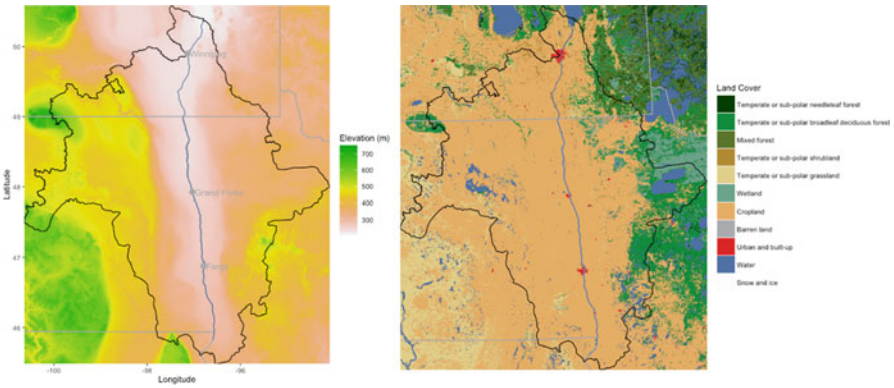

Fig. 2.2 Terrain (*left*) (from the ETOPO1 global relief model; Amante and Eakins 2009) and land cover (*right*) (NALCMS 2015) of the Red River of the North basin (excluding the Assiniboine River basin). The basin has very low relief and is dominated by cropland

River is approximately 885 km long and with a drainage area of 285,000 km^2 (including the 162,000 km^2 Assiniboine drainage), about 635 km and 101,500 km^2 of which are in the United States, respectively (Rannie 2016; Miller and Frink 1984). Along this distance, the main stem of the Red River drops only 72 m, for an average grade of 0.08 m/km. This lack of relief (Fig. 2.2) is one of the river's main features and partly helps to explain why the region is so vulnerable to flooding.

Spring snowmelt floods are a regular occurrence in the Red River of the North basin. Approximately 85 % of the yearly maximum peak flows in the RRB over the past century resulted from the spring melt, as opposed to only 15 % from summer or fall rain-driven events (Rasmussen 2016, Fig. 2.3). Despite the low average SWE compared to mountain snowpacks (Sturm et al. 1995; Brasnett 1999), spring floods in the Red River basin persist on a timescale of weeks to months (e.g., the Red River exceeded flood stage in Grand Forks, ND for 46 days during the record-breaking 1997 flood; Todhunter 2001) and floodwaters can extend for large distances from the main channel (e.g., flood width of up to 80–100 km near the U.S.–Canada border; Schwert 2003; Miller and Frink 1984).

In recent decades, the Red River experienced a number of large flood events (Fig. 2.3), including the aforementioned 1997 snowmelt flood. More recently, the 2009 spring flood included the highest ever river stage recorded at Fargo, ND, forcing evacuations and inundating hundreds of homes (Wazney and Clark 2016; Rogers et al. 2013), while the 2011 flood was the third-highest stage ever recorded at Grand Forks, ND (Stadnyk et al. 2016). It has been suggested that the increase in Red River flooding could be due to human-induced climate change, but the region is subject to multidecadal oscillations from very wet to dry periods (Knox 2000; Miller and Frink 1984; see Fig. 2.3), making causal attribution challenging (Hirsch and Ryberg 2012; Rasmussen 2016). Another possible explanation for the increase in flooding is change in agricultural practices, including extensive ditching and installation of subsurface drainage (Miller and Frink 1984) (e.g., Bois de Sioux

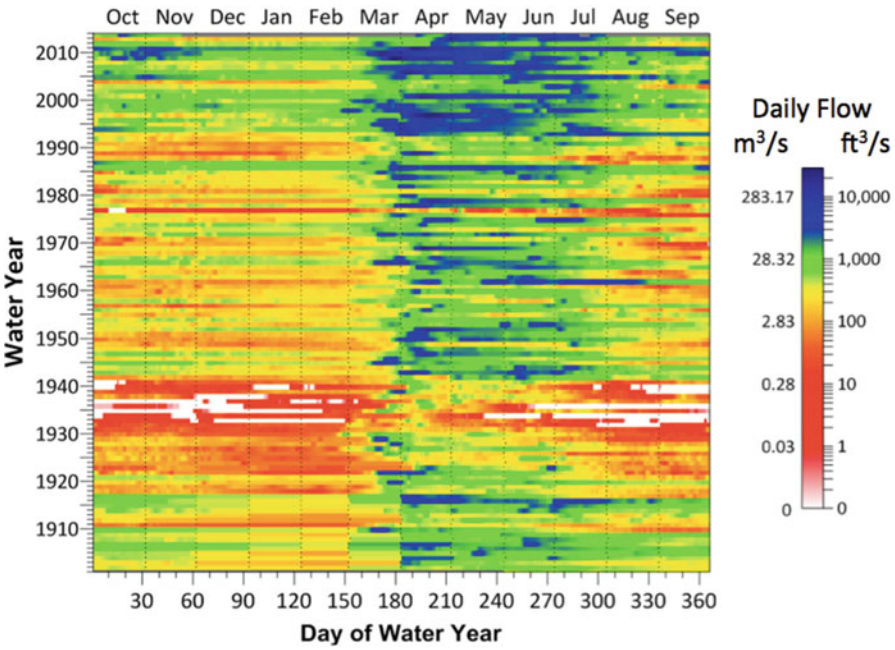

Fig. 2.3 Plot of daily Red River discharge at Fargo, ND (USGS gage 05054000) as a function of water year and day of water year (courtesy of Richard Koehler, NOAA NWS). Blue colors indicate high flows and red colors indicate low flows. Most of the highest flows occur from March to July, as a result of the spring snowmelt. The 1930s–1940s was a very dry period, while flows have increased in recent decades

Watershed District tile permit growth map: http://www.frontiernet.net/~bdswd/Files/Tile_Permit_Growth_Map_Reduced.pdf). However, it is difficult to isolate the effect of the man-made changes to peak river flows (Miller and Frink 1984; Rahman et al. 2014).

Despite the frequency of flooding in the region, ground observations of hydrological state variables are relatively sparse compared to other regions of the United States. Currently, frequent, high quality ground-based measurements of SWE and soil moisture are available from less than 20 and 10 locations, respectively, in the U.S. portion of the basin. This scarcity of SWE and soil moisture makes flood forecasting difficult in the Red River, but remote sensing can increase the spatial and temporal coverage of observations. Two issues that complicate satellite estimates of snow and soil moisture—rugged, steep terrain, and dense vegetation—are almost entirely absent from this region. The area is classified as 79 % cropland, 8 % grassland, shrubland, or wetland, and only 9 % is any type of forest (NALCMS 2015; Fig. 2.2). The minimal topographical relief is evident in Fig. 2.2. Due to these factors, remote sensing can be helpful to constrain hydrologic states that are important for accurate flood forecasting.

2.3 Snow Water Equivalent

SWE is the depth of liquid water that would result if the entire snowpack (at any given time and location) melted. Accurate flood forecasting requires knowledge of the magnitude and spatial distribution of SWE within a given basin. Remote sensing, especially passive microwave methods, can provide estimates of SWE and thus help to constrain this primary driver of spring flooding in areas such as the Red River of the North basin.

2.3.1 Passive Microwave

Most research in satellite remote sensing of SWE has focused on microwave frequencies, and specifically passive microwave radiometers. Passive microwave sensors detect the natural thermal emission of microwave radiation from the earth's surface. The primary instruments used for this purpose are listed in Table 2.1.

Multiple algorithms were developed over the past three decades to convert passive microwave brightness temperatures to depth and water equivalent of dry snow, beginning with Chang et al. (1982, 1987). The widely used "Chang algorithm" approach (and its later variants, e.g., Chang and Rango 2000; Kelly 2009) exploits the fact that higher frequency microwave radiation emitted from the earth's surface is scattered by snow particles, while snow is more transparent to microwaves at lower frequencies. Generally, the greater the snow depth, the greater the scattering, and the lower the detected brightness temperature, for a given snowpack temperature (Ulaby and Stiles 1980). Thus, passive microwave methods technically observe the effect of snow depth on thermally emitted radiation, so conversion of inferred snow depth estimates to SWE requires assumption of grain size and density (e.g., from Sturm et al. 1995, 2010). Chang et al. (1987) used the difference between brightness temperatures at 37 and 18 GHz frequencies (i.e., the "spectral gradient") of the SMMR satellite instrument and calibrated a simple linear coefficient to convert the brightness temperature difference to SWE, using an assumed snow density and grain size (Davenport et al. 2012). This approach was later modified for the SSM/I series of satellite instruments, and expanded to include more frequencies, and forest fraction and grain size corrections, for the current operational AMSR-E and AMSR2 algorithms (Kelly 2009). Other authors developed a modified "Chang" algorithm that further accounts for snow morphology over the course of the winter (Josberger and Mognard 2002).

In the past 15 years, new algorithms branched out beyond "Chang" methods, such as an algorithm based on the dense media transfer model (DMRT) (Kelly et al. 2003), which may soon be implemented as the operational AMSR2 algorithm (Richard Kelly, University of Waterloo, personal communication). Tedesco et al. (2004) developed an algorithm based on artificial neural networks, which compared well to other methods, especially when trained using experimental data.

Table 2.1 Passive microwave satellite sensors for SWE and soil moisture

Instrument	Satellite platform	Agency	Relevant frequencies (GHz)	Product spatial resolution	Temporal resolution	Operational period
Snow water equivalent						
AMSR2	GCOM-W1	JAXA	10.65, 18.7, 36.5, 89	10, 25 km	1–2 day	2012–present
AMSR-E	Aqua	NASA	10.65, 18.7, 36.5, 89	25 km	1–2 day	2002–2011
SSM/I and SSMIS	DMSP (multiple)	DoD	19.35, 37.0	25 km	1–2 day	1987–present
SMMR	Nimbus-7	NASA	18.0, 37.0	25 km	2–6 day	1978–1987
Soil moisture						
SMAP	SMAP	NASA	1.4	36 km	2–3-day	2015–present
AMSR2	GCOM-W1	JAXA	6.9, 10.65	25 km	1–2 day	2012–present
Aquarius	SAC-D	NASA	1.4	1 deg.	0.5–1 week	2011–2015
SMOS/ MIRAS	Proteus	ESA	1.4	25 km	2 day	2009–present
AMSR-E	Aqua	NASA	6.9, 10.65	25 km	1–2 day	2002–2012
SSM/I and SSMIS	DMSP (multiple)	DoD	19.35	25 km	1–2 day	1987–present
SMMR	Nimbus-7	NASA	6.6, 10.7	25 km	2–6 day	1978–1987

AMSR2 Advanced Microwave Scanning Radiometer 2, *GCOM-W1* Global Change Observation Mission—Water "Shizuku," *JAXA* Japanese Aerospace Exploration Agency, *AMSR-E* Advanced Microwave Scanning Radiometer for EOS, *NASA* National Aeronautics and Space Administration, *SSM/I* Special Sensor Microwave Imager, *SSMIS* Special Sensor Microwave Imager/Sounder, *DMSP* Defense Meteorological Satellite Program, *DoD* U.S. Department of Defense, *SMMR* Scanning Multichannel Microwave Radiometer, *SMAP* Soil Moisture Active Passive, *SAC-D* Satélite de Aplicaciones Cientificas-D, *SMOS* Soil Moisture and Ocean Salinity, *MIRAS* Microwave Imaging Radiometer with Aperture Synthesis, *ESA* European Space Agency

Other authors tested algorithms that use artificial neural networks, projection pursuit regression, general linear models, and nonlinear regression (Josberger et al. 1998; Singh and Gan 2000; Gan et al. 2009), but Chang-type methods remain in use as the primary algorithms for AMSR-E and AMSR2. Recent SWE products assimilate remote sensing and ground observations into computer models, including the Finnish Meteorological Institute (FMI)-led Global Snow Monitoring for Climate Research (GlobSnow) database (Luojus et al. 2013; Takala et al. 2011; Pulliainen 2006). The combination of models and observations may help to mitigate some of the shortcomings of passive microwave methods. Fundamental physics of microwave remote sensing of snow were summarized by Ulaby et al. (1981), Hallikainen et al. (1986), Mätzler (1987), Hallikainen (1989), and Chang et al. (1975). Rango (1993), Hall et al. (2006), and Dietz et al. (2012) provided reviews of snow remote sensing methods, while Clifford (2010) and Frei et al. (2012) reviewed global snow products.

Some of the earliest studies to examine the potential of microwave radiometers to detect snow took place in the northern Great Plains (e.g., Foster et al. 1980). Josberger et al. (1998) explored alternative methods (multiple linear regression, neural networks, and general linear models) to extract SWE from SSM/I microwave observations. Singh and Gan (2000) tested multiple "Chang-type" algorithms for use with SSM/I observations, also in the Red River basin. Foster et al. (2001) tested Chang et al. (1987) algorithm estimates of snow depth from SSM/I, modified for snow grain size and forest fraction, against ground observations of snow and gamma-derived snow depth estimates in the Roseau River basin, finding high correlation. Josberger and Mognard (2002) developed a Chang-type snow depth algorithm that uses air temperature to calculate a temperature gradient index as a proxy for snow grain metamorphism and applied it to SSM/I observations in the northern Great Plains. Mognard and Josberger (2002) examined the performance of the temperature gradient index algorithm in the region during the 1996/1997 snow season, finding that their dynamic algorithm agreed well with ground observations but algorithms that assume a constant grain size led to underestimation of snow depth (presumably due to underestimation of grain size). Mote et al. (2003) compared SWE from the SNTHERM model, the SSM/I SWE algorithm, and in situ measurements from five stations in the northern Great Plains, finding that the model underestimated SWE and the microwave algorithm overestimated SWE in late winter, likely due to metamorphism and grain growth. Dong et al. (2005) examined sources of uncertainty in SMMR Chang algorithm SWE across Canada using SWE derived from in situ snow depth observations, which indicated that the dominant errors in remotely sensed SWE are due to saturation of the microwave signal at high snow depth, high air temperature, and proximity to large water bodies. Chang et al. (2005) explored the uncertainties in point-based ground data as compared to larger scale SSM/I satellite estimates in the northern Great Plains. The authors found some significant differences between the two estimates in yearly snow depths but insignificant differences using the 10-year mean, and emphasized that approximately ten points measurements are necessary to produce a sampling error of 50 mm in 1° by 1° grid cells. Using airborne gamma radiation SWE estimates as "truth," Gan et al. (2009) compared an artificial neural network method of estimating SWE from SSM/I brightness temperature observations to projection pursuit regression and nonlinear regression methods in the Red River basin, finding that the neural network method was superior to the other two methods. Clearly, the northern Great Plains has been a test bed for developing and evaluating satellite SWE algorithms.

SWE remote sensing studies specific to the Red River basin decreased in recent years, but some other larger-scope analyses are worth noting, given their relevance to the use of passive microwave SWE estimates for flood forecasting. Vuyovich and Jacobs (2011) compared SSM/I and AMSR-E SWE estimates to a temperature index snow model driven by Tropical Rainfall Measuring Mission (TRMM) precipitation estimates in central Afghanistan and found that the satellite estimates were comparable but of higher magnitude than the modeled SWE for some winters. This analysis indicated that updating the snow model with satellite SWE estimates

considerably improved modeled runoff and reservoir storage predictions and noted that rain on snow events is detectable in microwave observations as sharp decreases in SWE. Vuyovich et al. (2014) compared SSM/I and AMSR-E SWE estimates to NOAA NWS Snow Data Assimilation System (SNODAS) estimates in watersheds across continental United States, finding that the best agreement was for basins with less than 200 mm maximum annual SWE and forest fraction less than 20 %. Hancock et al. (2013) compared SSM/I, AMSR-E, and GlobSnow SWE estimates to remotely sensed snow covered area (SCA), in situ ground observations, and meteorological data across the northern hemisphere. The authors found that SSM/I and AMSR-E SWE estimates saturated in high snow covers, showed spurious spikes at the onset of spring melt, and overestimated under cold air temperatures and in forested areas, indicating that GlobSnow more accurately determines peak SWE accumulation and the seasonal appearance and disappearance of snowpack.

Analyses by the authors of this chapter suggest that passive microwave SWE estimates compare reasonably well to other observations in the northern Great Plains (e.g., Fig. 2.4). The root mean square error (RMSE) between AMSR-E SWE and 1172 U.S. Army Corps of Engineers (USACE) St. Paul District ground-snow-survey SWE observations taken between 2002 and 2011 is 34.7 mm with a coefficient of determination (R^2) of 0.36. This error is moderate, but the bias was only −3.8 mm, indicating that most of the error is likely due to the scale difference between point surveys and 25 km satellite pixels, along with the considerable variability of snow depth in the region (Chang et al. 2005; Cork and Loijens 1980).

The aforementioned research articles and further observations by the authors of this chapter emphasize important limitations of passive microwave SWE estimates (also discussed by Tedesco and Narvekar 2010):

1. For the wavelengths used by current satellites, the lower frequency microwave channels cannot penetrate deep snow covers, leading the SWE estimates to saturate at high snow depths. This is not a frequent concern for the Northern Great Plains due to its limited snowfall compared to mountainous regions.
2. The physics of wet snow are different than for dry snow. Wet snow favors absorption of microwave radiation rather than scattering, and thus, SWE retrieval is not feasible in the presence of liquid water. While microwave observations from wet snow change somewhat with increasing liquid water content (Kang et al. 2014), generally wet snow causes the brightness temperatures at different microwave frequencies to converge and thus leads the Chang-type SWE algorithms to estimate zero snow depth. Vuyovich et al. (2014) used the weekly maximum SWE to minimize impacts of wet snow on SWE estimates.
3. Accurate characterization of grain size and snow density throughout the winter is crucial for accurate SWE estimates. Snow metamorphosis over the course of the winter results in grain size and density increases (Bader et al. 1939; Colbeck 1982; Josberger and Mognard 2002), which can disproportionately decrease emitted microwave radiation. Increased attenuation at higher frequencies increases the temperature brightness differences and, without correction, makes the snow seem deeper than it is in reality (e.g., Chang et al. 1987,

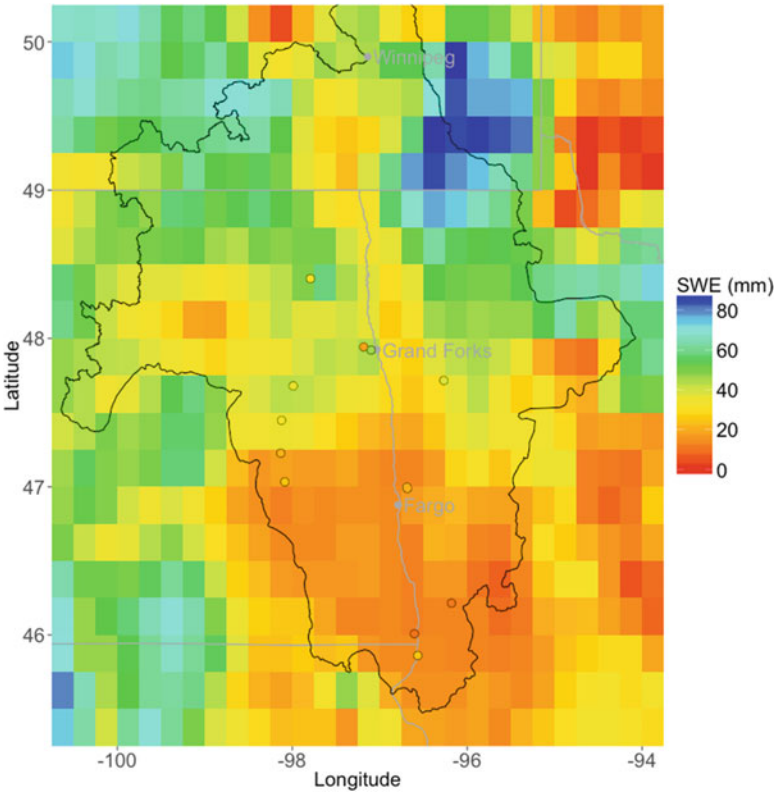

Fig. 2.4 Example comparison of AMSR2 passive microwave satellite SWE estimates to in situ ground observations, shown using the same color scale. The ground observations were collected between January 21 and 27, 2016, and the AMSR2 SWE (raster grid) is averaged over that period. A majority of the ground measurements are from manual snow tube surveys, but one point is from a snow pillow. The in situ and satellite estimates agree quite well, given the large disparity in observation scale, but the satellite may slightly overestimate SWE in the northwest RRB

Fig. 2.1). Thus, an algorithm that assumes a constant snow grain size and density will often underpredict SWE in early winter (when the grain size is small and density is low), and overpredict in the late winter (when the grain size is large and density is high). Changing snow properties and ice formation during melt-refreeze in early spring may also explain the spurious spikes in SWE observed by Hancock et al. (2013). In prairie environments such as the Red River basin, snowpacks are often shallow and air temperatures well below freezing, which can lead to the formation of large, platy crystals within the snowpack called depth hoar (Bader et al. 1939; Giddings and LaChapelle 1962), so accurate grain size estimates are crucial for accurate SWE estimates in this region.

4. Dense vegetation can inhibit accurate retrieval of SWE, but this is not a major concern for the cropland-dominated Red River basin.

Atmospheric effects also attenuate the microwave signal, but seasonal variation in this effect is negligible, and it may only be important during cloudy conditions (Wang and Tedesco 2007). For low relief, low vegetation watersheds such as the Red River basin, passive microwave SWE estimates provide the most value from early winter until snowmelt onset. Awareness of when and how snowpack physical conditions impact retrievals can optimize the useful information on SWE depth and spatial variability provided by passive microwave SWE observations. While there is still room for improvement in the global SWE algorithms, specific regional products or QA/QC analyses are an alternative approach to improving flood forecasting skill using microwave remote sensing.

2.3.2 Airborne Gamma Radiation Surveys

The potential use of natural terrestrial gamma radiation to estimate SWE for flood forecasting applications was recognized by the National Weather Service (NWS) in the late 1960s (Peck et al. 1971). Gamma radiation is naturally emitted from radionuclides in soil, including uranium, potassium, and thorium, and radiation from approximately the top 20 cm of the soil can be detected above the land surface (Carroll and Schaake 1983; Carroll 2001). However, water in any phase will attenuate gamma radiation, so the amount of gamma radiation reaching a detector from a bare soil is greater than that from the same soil when it is snow covered. The difference in radiation is proportional to the amount of SWE (i.e., mass of water; Peck et al. 1971).

Much of the North American-based research on airborne measurement of SWE using gamma radiation was conducted in the 1970s–1980s, and focused on "ground truthing" the data using ground measurements of SWE and snow depth, along with the correction for the effects of soil moisture, background radiation (e.g., from the aircraft and cosmic sources), atmospheric radon, Compton scattering, and air density on the gamma radiation signal (Peck et al. 1971, 1980; Carroll and Schaake 1983). Additional studies attempted to quantify the effect of uneven snow cover (e.g., from drifting; Cork and Loijens 1980; Carroll and Carroll 1989b) and vegetation (Carroll and Carroll 1989a) on the gamma radiation SWE estimates. During this time, researchers developed approaches to use the gamma radiation counts to estimate SWE, including single-flight methods that used the shape of the gamma spectra to infer SWE (Grasty 1982), and two-flight methods that include a calibration flight over bare soil in the fall (Carroll and Schaake 1983; Carroll 2001).

In 1980, the NWS set up an operational network of gamma radiation flight lines in the north central region on the United States, which now consists of over 2400 flight lines in 29 states and seven Canadian provinces. Each flight line is approximately 15–20 km long with a width of approximately 330 m. Thus, the areal coverage of each flight line is approximately 5–7 km^2. Currently, NOAA's National Water Center (NWC) maintains the flight line network and measures it each winter in support of river forecasting centers such as the North Central River Forecast

Center (NCRFC) (data freely available on http://www.nohrsc.noaa.gov/snowsurvey/).[1] The NWS opted for the two-flight method, utilizing the gamma radiation counts for the ^{40}K and ^{208}Tl photopeaks, and the total count between 0.41 and 3.0 MeV to obtain a single weighted estimate of SWE (Carroll and Schaake 1983; Carroll 2001). During the fall, gamma radiation for each flight line is measured over snow-free soil at a height of 150 m, in order to obtain a baseline estimate of soil moisture (Carroll 2001). The difference in gamma radiation measured between the fall flight and any subsequent identical flights over winter snowpack reflects the amount of SWE on the ground (as well as any potential changes in soil moisture status). Each year, the NWC obtains SWE estimates from zero to four times per line, depending on the presence of snow and flooding potential of the region.

Previous studies indicate that airborne gamma radiation techniques estimate SWE with an RMSE of 8.8 mm and an average bias of +54 mm (Carroll and Schaake 1983). NWC gamma radiation SWE estimates have become an important supplemental source of information for flood forecasting in the Red River basin (Brian Connelly, NCRFC, personal communication). A strength of the gamma estimates is that they are unaffected by the phase of water on the ground; the attenuation of gamma radiation is only dependent on the mass of water on the ground surface (e.g., dry snow, wet snow, ice, ponded water, etc.) and in the top 20 cm of soil. However, spatial coverage (only 5–7 km^2 per flight line) and logistics (limited aircraft flight time over the course of the winter season) limit the usefulness of the gamma flights. Also changes in below-ground water content during the winter can lead to inaccurate SWE estimates, as the gamma radiation method is affected by all water above approximately 20 cm depth.

In summary, it is challenging to capture the magnitude and variability of SWE at the spatial and temporal scales necessary for operational flood forecasting. Even the most trusted SWE observations from in situ surveys can be subject to undersampling errors (Carroll 2001) and lack the sampling density to characterize the considerable spatial variability of SWE in the region (Chang et al. 2005). Passive microwave and airborne gamma radiation methods provide complementary SWE estimates (Fig. 2.5). While gamma radiation observations have a proven track record for operational flood forecasting, microwave products appear to be of good enough quality to be informative. For these methods, validation from in situ observations, and even an intercomparison between the two remote sensing observations, is difficult because the spatial properties of the different measurement techniques are not the same. Microwave SWE algorithms continue to evolve to improve global retrieval performance. However, operational users of these products would be well served by an understanding of how products perform under the different snow conditions within their forecast region.

[1] Until recently, the flight line network was maintained by the NOAA NWS National Operational Hydrologic Remote Sensing Center (NOHRSC) in Chanhassen, Minnesota, before it became a part of the National Water Center (NWC).

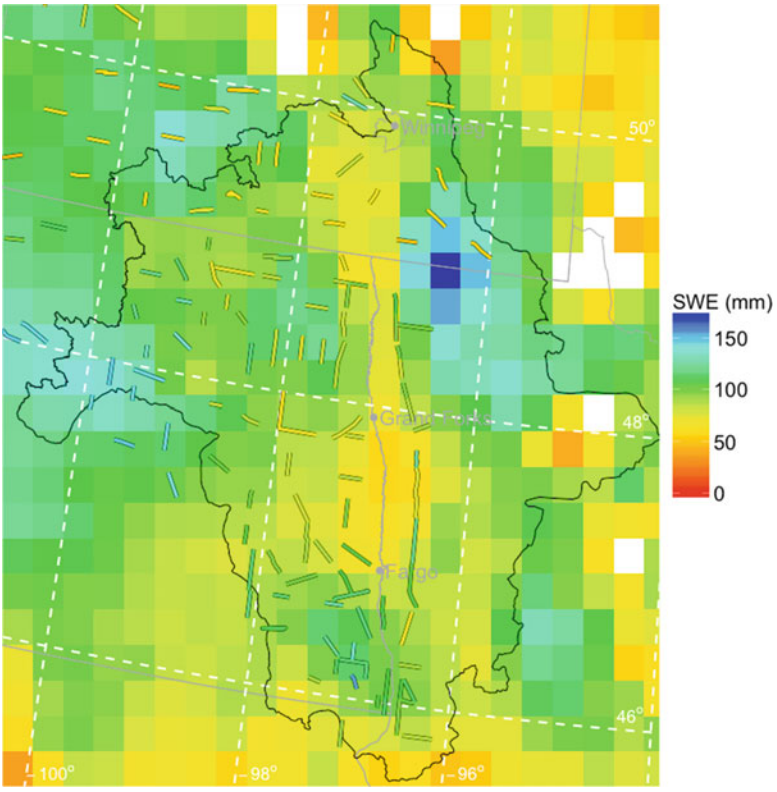

Fig. 2.5 Comparison of SWE estimated from NOHRSC airborne gamma radiation surveys and AMSR-E descending overpasses, shown on the same color scale. The gamma radiation surveys (*colored lines*) were conducted between March 11 and 14, 2009, and the AMSR-E SWE (raster grid) is averaged over that period. The gamma radiation and passive microwave estimates agree quite well, given the difference in measurement depths and footprint size

2.4 Soil Moisture

Fall soil moisture is important for spring flooding because it determines the partitioning of snowmelt between infiltration and runoff. Drier soil has a greater available water storage capacity. In areas with winters where air temperatures often remain well below freezing, such as the north central United States, soils regularly freeze in late fall and do not thaw until the spring (Todhunter 2001). This means that the soil water content in the fall becomes locked in the frozen soil and remains relatively constant until the following spring thaw. Thus, the soil wetness in late fall plays a role in determining the severity of spring flooding because drier soils are able to store more meltwater the following spring, as compared to wetter soils, resulting in less runoff. While the broader Great Plains region has a rich history as a test bed for microwave remote sensing of soil moisture, relatively few studies have

been conducted in the Red River basin. These are summarized in the following sections, along with relevant studies from other nearby regions.

2.4.1 Passive Microwave

Remote sensing of soil moisture provides value for drought monitoring, agriculture, climate change, and land–atmosphere interactions. While active microwave satellite sensors (e.g., the Advanced Scatterometer (ASCAT); Wagner et al. 2013) can also observe soil moisture, passive microwave sensors are more numerous and have a more robust validation history. Many of the same sensors used for SWE estimation are also used for soil moisture estimation (see Table 2.1). While SWE algorithms utilize microwave measurements in the 10–89 GHz range, soil moisture remote sensing focuses on lower 1–10 GHz frequencies due to the greater penetration of those frequencies into the soil (1–5 cm) and greater transmissivity through vegetation. Older sensors operated at higher frequencies (e.g., SMMR, SSM/I, AMSR-E: 6–11 GHz), but newer sensors have trended toward lower frequencies (e.g., SMOS, SMAP: 1.4 GHz), allowing greater observation depths.

While some snow algorithms are relatively simple (e.g., Chang et al. 1987), soil moisture algorithms must account for the effects of surface temperature, vegetation, soil roughness, and soil dielectric properties on the thermal emission of microwave radiation in order to estimate soil moisture (Njoku and Entekhabi 1996). Generally, soil moisture algorithms use empirical relationships to determine the emissivity from a soil–water mixture, and modify the emissivity for the effects of soil roughness and vegetation. Due to this complexity, many algorithms employ an inverse modeling approach (as compared to the forward approach for SWE) to relate brightness temperature observations to soil moisture estimates (e.g., Jackson 1993; Owe et al. 2001; Njoku et al. 2003; Jones et al. 2009; Kerr et al. 2012; Santi et al. 2012).

Numerous remote sensing field validation campaigns have been conducted across the United States including Oklahoma (SGP97, SGP99, SMEX03, CLASIC07), Iowa (SMEX02, SMEX05), Georgia (SMEX03), Alabama (SMEX03), Arizona (SMEX04, SMAPVEX15), and Maryland (SMAPVEX08) (e.g., Colliander et al. 2012). Despite the relatively flat, low vegetation landscape of the northern Great Plains, presumably ideal for passive microwave remote sensing, no campaigns have taken place in North or South Dakota, or Minnesota (however, SMAPVEX12 was conducted west of Winnipeg, Canada in the Assiniboine River basin, and CanEX-SM10 was in the neighboring Saskatchewan). Most campaigns have coincided with experimental watersheds or other well-instrumented areas. The Red River basin (and the northern Great Plains in general; see Fig. 2.1) notably lacks in situ soil moisture measurements that could assist in validation and flood forecasting.

While soil moisture in the Red River basin appears to be understudied, passive microwave remote sensing has proven successful in more southern areas of the

Great Plains. Jacobs et al. (2003) provided an early demonstration of the potential value of remotely sensed soil moisture to improve rainfall-runoff predictions, using observations from the Oklahoma SGP97 experiment. Jackson et al. (2010) validated estimates from multiple AMSR-E soil moisture algorithms against in situ measurements in four research watersheds (Little Washita, OK; Reynolds Creek, ID; Little River, GA; and Walnut Gulch, AZ), finding a wide range of performance across algorithms. Two of the four tested algorithms met the NASA AMSR-E mission's 0.06 $m^3\ m^{-3}$ RMSE requirement at the Oklahoma site, and simple bias and regression corrections yielded standard errors of 0.04–05 $m^3\ m^{-3}$ for all four algorithms. A similar study (Jackson et al. 2012) validated SMOS soil moisture estimates, indicating an RMSE of approximately 0.043 $m^3\ m^{-3}$ and near-zero bias for the Oklahoma site. Leroux et al. (2016) examined the performance of a prototype SMAP algorithm over a challenging, wide range of vegetation and soil conditions using airborne observations from the PALS instrument during the Manitoba, Canada SMAPVEX12 campaign, finding that soil moisture errors ranged from 0.05 to 0.1 $m^3\ m^{-3}$.

Additional comparisons by the authors of this chapter show that L-band (1.2 GHz) passive microwave soil moisture products are promising for flood forecasting applications. Preliminary SMAP Level 3 results in the Red River basin show that the RMSE is 0.059 $m^3\ m^{-3}$, with a bias of $-0.011\ m^3\ m^{-3}$ (and Kendall's τ rank correlation coefficient of 0.578), when evaluated against daily-averaged in situ soil moisture from 5 cm depth at the Glacial Ridge, MN SCAN site (Fig. 2.6; Schaefer et al. 2007). This comparison ignores the considerable spatial difference between the "point" measurements and gridded 36 km resolution satellite estimates, which is likely a significant source of error. SMOS estimates from

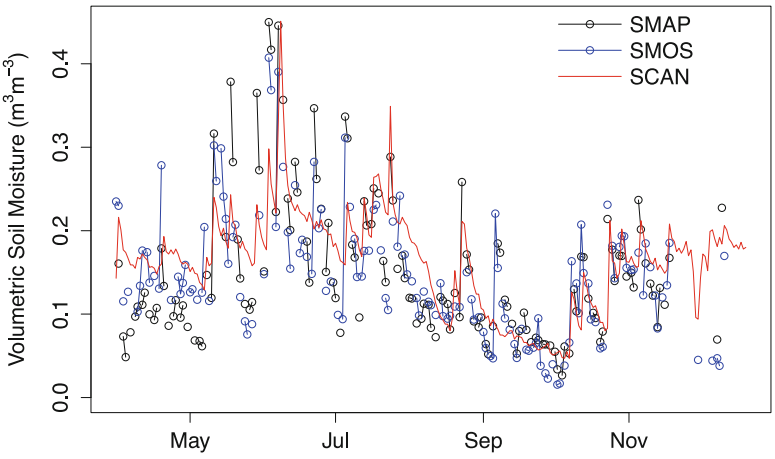

Fig. 2.6 Time series of 5 cm depth soil moisture at the Glacial Ridge, MN SCAN site (*red*) from April to December, 2015, along with passive microwave satellite estimates from SMAP (*black*), SMOS (*blue*). The SMAP and SMOS estimates agree quite well with the in situ observations, despite the large difference in observation scales

2015 also compare favorably to in situ SCAN data, with an RMSE of 0.054 $m^3\ m^{-3}$ and bias of $-0.013\ m^3\ m^{-3}$ (and Kendall's τ of 0.513). However, the comparison is not as encouraging for other products from older instruments that operate at higher frequencies (e.g., AMSR2 with LPRM algorithm: RMSE = 0.188 $m^3\ m^{-3}$, bias = 0.124 $m^3\ m^{-3}$, Kendall's $\tau = -0.017$).

Similar to SWE estimates, remotely sensed soil moisture has the ability to resolve the spatiotemporal evolution of the ground state. Figure 2.7 shows an example of a late fall soil moisture map from SMAP. The map clearly shows the relatively dry conditions prior to the fall-winter transition, especially in the southern portion of the Red River basin, although in situ observations suggest that SMAP estimates may be biased low for finer RRB soils. The Red River clay soils can develop large cracks under drought conditions, which serve as preferential drainage pathways. SMAP soil moisture estimates can potentially identify when cracking is likely to occur. Thus, the remote sensed soil moisture product has value to flood

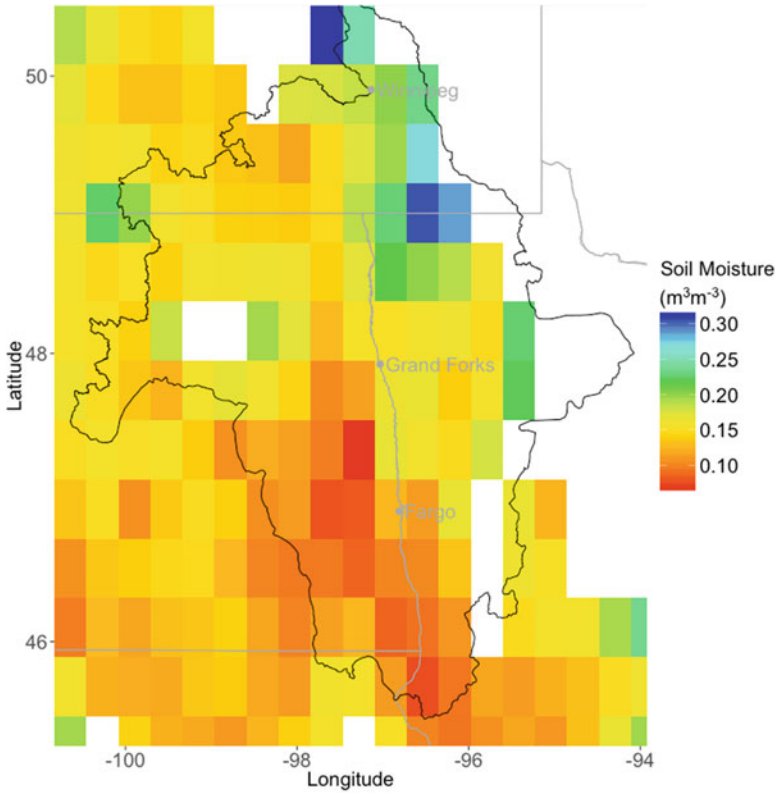

Fig. 2.7 Late fall soil moisture from SMAP (Level 3 product). The values shown are the mean soil moisture from November 15 to 28, 2015. The data were screened for the presence of open water (>10 % of pixel area), dense vegetation, precipitation, and snow or ice using SMAP data quality flags

forecasting centers for initializing operational models before the winter freeze-up and may provide insight into infiltration rates. In summary, comparisons between in situ and passive microwave estimates suggest that current satellite sensors can provide soil moisture estimates sufficient for operational use in flood forecasting, although some calibration may be necessary for finer soils.

2.4.2 Additional Soil Moisture Remote Sensing Methods

While passive microwave remote sensing has a strong history of performance in the Great Plains, the large spatial scale and relatively shallow depth of the soil moisture observations makes operational use of the products challenging in smaller basins. There are a number of additional airborne and satellite instruments which can provide observations to support the characterization of antecedent soil moisture conditions.

In addition to SWE estimations, airborne gamma radiation surveys produce estimates of soil moisture in the upper 20 cm of soil. Jones and Carroll (1983) and Carroll and Schaake (1983) summarize the method used to estimate soil moisture from gamma radiation observations, which is based on the difference in gamma radiation flux measured over dry and wet soils. The NWC estimates soil moisture for each flight line by obtaining gamma radiation observations in coincidence with gravimetric soil moisture samples (approximately 25 per 16–20 km flight line), yielding an empirical historical relationship. An early study of 155 flights over 42 flight lines found that the RMSE between in situ and airborne gamma radiation soil moisture is 0.039 $m^3\ m^{-3}$ soil moisture with an average bias of 0.001 $m^3\ m^{-3}$ (Jones and Carroll 1983). The NWC surveys the flight line network over bare soil approximately 1–2 times per fall (http://www.nohrsc.noaa.gov/snowsurvey/soil.html).

Rijal et al. (2013) explored the potential to use Landsat 5 TM data to detect soil moisture in the laboratory and field, at a much higher resolution (30 m) than passive microwave estimates (25–36 km). However, optical reflectance only observes soil moisture at skin depth, and thus relies on correlation with depth in order to estimate deeper soil moisture. For this reason, the authors used an empirical relationship to relate optical reflectance to soil moisture. The authors found an encouraging average difference of 0.02 $cm^3\ cm^{-3}$ between 15 cm depth estimated and field-measured soil moisture, but cautioned that their model should not be used elsewhere without validation. This method could show promise for providing soil moisture at the property scale with fair temporal resolution, which is not currently feasible using other methods.

As mentioned earlier, active microwave instruments also have a strong potential to provide high quality soil moisture estimates (e.g., ASCAT; Wagner et al. 2013). Additionally, Liu et al. (2011) created a multisensor soil moisture climatology that incorporates observations from both passive and active instruments starting in 1978 and currently extends through 2014, which could be useful for retrospective model testing.

2.5 Remote Sensing Data and Operational Flood Forecasting Models

While remote sensing observations have tremendous potential to inform antecedent moisture and snowpack states, translation to improved flood forecasting is not necessarily straightforward. In order for remote sensing data to be useful for operational flood forecasting, the data must (1) be trusted by the forecasters, and (2) successfully integrate into the flood modeling workflow. These points may seem trivial, but flood forecasting centers have established "tried and true" procedures. New datasets must demonstrate additional value beyond the current capability of the modeling system before they will be adopted into the forecasting workflow.

For example, the NOAA National Weather Service North Central River Forecast Center is responsible for forecasting river flows at 447 forecast points across the Upper Mississippi, Great Lakes, and Hudson Bay drainages at a 6-hourly time step. Briefly, the NWS hydrologic operational forecasting modeling system, the Community Hydrologic Prediction System (CHPS),[2] links the SNOW-17 snow model (Anderson 2006) to the Sacramento Soil Moisture Accounting (SAC-SMA) model (Burnash 1995) to a number of hydrologic and hydraulic flow routing models. The primary inputs to the model are mean areal temperature and precipitation from observations and NWS forecasts, and the main output is river discharge (and stage). The modeling system is lumped, with the watershed divided into many subbasins, and the NCRFC calibrates and runs the model at the subbasin scale. During operational forecasting, the NCRFC forecaster runs the model and obtains a river flow prediction, which is compared to observed streamflow at U.S. Geological Survey (USGS) streamgage locations. The forecaster then uses professional judgment to either accept the forecast, or to modify one or more model states and rerun the model, which will then change the predicted river flows. For instance, if the model has predicted a higher river discharge than the observed USGS streamflow for the past few time steps, the forecaster may decide to increase the model SWE to effectively reduce the meltwater routed to the stream, in order to better match the observations. In this case, the passive-microwave-derived SWE product might be well suited to help the forecaster understand variations across the watershed.

The current operational procedure does not have an established approach to assimilate observational data into the model. Furthermore, modeled streamflows depend on both model processes and model states, so streamflow prediction errors can arise from either source. Forecasters can compensate for deficiencies of the model by making manual changes, and most changes are based on observed streamflow rather than observed snow or soil moisture. These modifications may sometimes move the modeled states closer to "reality," but in other cases, forecasters may make adjustments to model states that appear to contradict observations, but lead to better river forecasts. Due to the latitude given to the forecasters in

[2] http://www.nws.noaa.gov/oh/hrl/general/indexdoc.htm

model modification, remote sensing data will not be incorporated into the modeling procedure unless the forecasters find that it provides value to improving the streamflow predictions. For this reason, an early step toward incorporation of remotely sensed data in operational modeling is to make the data readily available, so that the forecasters can visualize it during their normal modeling procedure and gain familiarity with its strengths and weaknesses.

A second consideration for the use of remotely sensed data in operational flood forecasting is how the remote sensing data maps to the model variables. The physical dimensions and units of model states may not match those from available remotely sensed observations. For instance, SAC-SMA is a "bucket" model. Its soil moisture domains have a defined maximum depth of water (determined separately for each watershed via calibration), but no specified depth into the ground. Remote sensing estimates of soil moisture, on the other hand, provide a volumetric measure of soil moisture which reflects all soil moisture in a given soil depth range. Thus, input of remote sensing estimates into operational models requires a keen understanding of the model states, the remotely sensed data, and the assumptions that underlie each dataset. Some methods have been developed to address translation of soil moisture fields into and between models (Koster et al. 2009), which include cumulative distribution function (CDF) matching (Reichle and Koster 2004), and data assimilation (Reichle 2008), but to date, there is no standard approach. In order to enable enhanced operational flood forecasting with remote sensing observations, facilitation of mutual understanding through communication between forecasters and remote sensing scientists is likely to be as important as high quality data.

2.6 Conclusion

In the northern Great Plains, great potential exists for remote sensing to contribute to operational flood forecasting by constraining drivers of spring snowmelt flooding. The region is generally flat with low vegetation cover, which makes it suitable for most remote sensing techniques. Many remote sensing methods have been tested in the region and proven useful in nearby areas (e.g., airborne gamma radiation surveys, passive microwave, optical, and radar satellite instruments), and current platforms provide readily available near-real-time data (e.g., SMAP, SMOS, and AMSR2 soil moisture, AMSR2 and SSM/I SWE). Remote sensing soil moisture estimates in the Red River appear to be sufficiently accurate for flood forecasting applications. SWE estimates show promise but users must be aware of the limitations of the data.

The northern Great Plains, especially Red River of the North basin, lack the necessary ground observations for accurate spatial characterization of snow water equivalent and soil moisture at the subbasin scale, which can be provided by remote sensing observations. However, additional ground instrumentation is needed in order to validate remote sensing products in the region and to inform flood forecasting. While additional SWE and soil moisture measurement sites are surely

necessary, observations of spring snow melting and ripening (which cannot be fully observed using passive microwave methods) are almost absent in the region, despite the importance of this time period for spring flooding. Additionally, snow grain size measurements, and more extensive snow density measurements, could help to improve SWE algorithms.

Flood forecasting and remote sensing in the northern Great Plains would also benefit from future field campaigns aimed to better understand snow and soil moisture processes in the region. Soil moisture field campaigns greatly outnumber snow campaigns over the past two decades. Snow campaigns hold great potential to advance the understanding of the region's hydrology. Such campaigns might benefit from an opportunistic, as opposed to scheduled, timeframe. Due to the yearly variability in weather and climate, it is difficult to determine when precipitation will occur, when snow will melt, etc., so it would be more effective to have a campaign ready for execution based on weather rather than planned dates.

While this chapter focuses on remote sensing methods used to estimate snow water equivalent and soil moisture, other exciting possibilities exist to remotely sense the drivers of spring snowmelt floods for use in operational flood forecasting. For instance, Ramage and Isacks (2002), Walker and Goodison (1993), and Grenfell and Putkonen (2008) developed methods to detect the presence of wet snow using passive microwave sensors. Snow covered area (SCA) from optical and infrared remote sensing (e.g., from the Moderate Resolution Imaging Spectroradiometer; MODIS) is considered to be a reliable method to observe snow cover extent and is already used operationally by some agencies (e.g., for hydropower generation in Norway; Winther and Hall 1999). The SMAP mission has produced a soil freeze–thaw product, while satellite instruments such as the Global Precipitation Measurement (GPM) mission (or ground-based radars such as the Next-Generation Radar (NEXRAD) network) can be used to detect spring precipitation. Synthetic aperture radar (SAR) and optical sensors (e.g., Landsat, MODIS, VIIRS) are useful for detecting river ice jams (Kreller et al. 2016). Additionally, during active flooding, remote sensing of flood heights may be obtainable with instruments such as the Surface Water Ocean Topography (SWOT) satellite mission, scheduled for launch in 2020. Finally, the extent of broad, slow-moving floods, such as those seen on the Red River, can be monitored using optical and infrared remote sensing (e.g., VIIRS, MODIS, Landsat; Wang et al. 2002; Zhan et al. 2002) or synthetic aperture radar (SAR; e.g., Wilson and Rashid 2005).

Improved snowmelt flood forecasts would immediately benefit large, vulnerable communities. Existing remote sensing tools provide a source of critically necessary information that can be made readily available to the forecasting community. Emerging remote sensing tools offer promise and, with further development, can complete the understanding of the significant changes in water and energy cycles throughout the entire winter and spring seasons.

Acknowledgements The authors gratefully acknowledge support from NASA Applied Sciences grant NNX15AC47G and NASA EPSCoR grant NNX11AQ34A. Additionally, thanks to Richard Koehler and Steven Quiring for allowing reproduction of their figures and data.

References

Amante C, Eakins BW (2009) ETOPO1 1 arc-minute global relief model: procedures, data sources, and analysis. NOAA Technical Memorandum NESDIS NGDC-24. National Geophysical Data Center, NOAA, Boulder

Anderson E (2006) Snow accumulation and ablation model–SNOW-17. US National Weather Service, Silver Spring

Anderson E, Larson L (1996) The role of snowmelt in the January 1996 floods in the northeastern United States. In: Proceedings of the 53rd Eastern Snow Conference, pp 141–149

Bader H, Haefeli R, Bucher E, Neher J, Eckel O, Thams C (1939) Snow and its metamorphism. In: U.S. Army Corps of Engineers (USACE) Cold Regions Research and Engineering Laboratory (CRREL) Snow, Ice, and Permafrost Research Establishment (SIPRE) Translation, vol 14. p 313

Beltaos S (2008) Progress in the study and management of river ice jams. Cold Reg Sci Technol 51 (1):2–19. doi:10.1016/j.coldregions.2007.09.001

Brasnett B (1999) A global analysis of snow depth for numerical weather prediction. J Appl Meteorol 38(6):726–740

Burnash RJC (1995) The NWS river forecast system—catchment modeling. In: Singh VP (ed) Computer models of watershed hydrology. Water Resources, Highlands Ranch, pp 311–366

Carroll T (2001) Airborne Gamma Radiation Snow Survey Program: a User's Guide, Version 5.0. National Operational Hydrologic Remote Sensing Center (NOHRSC), Chanhassen, p 14

Carroll SS, Carroll TR (1989a) Effect of forest biomass on airborne snow water equivalent estimates obtained by measuring terrestrial gamma radiation. Remote Sens Environ 27 (3):313–319

Carroll SS, Carroll TR (1989b) Effect of uneven snow cover on airborne snow water equivalent estimates obtained by measuring terrestrial gamma radiation. Water Resour Res 25 (7):1505–1510

Carroll TR, Schaake JC Jr (1983) Airborne snow water equivalent and soil moisture measurement using natural terrestrial gamma radiation. In: 1983 Technical Symposium East. International Society for Optics and Photonics, pp 208–213

Chang AT, Rango A (2000) Algorithm theoretical basis document (ATBD) for the AMSR-E snow water equivalent algorithm. NASA/GSFC, Nov 2000

Chang TC, Gloersen P, Schmugge T, Wilheit TT, Zwally HJ (1975) Microwave emission from snow and glacier ice. Ann Glaciol 16(74):23–39

Chang A, Foster J, Hall D, Rango A, Hartline B (1982) Snow water equivalent estimation by microwave radiometry. Cold Reg Sci Technol 5(3):259–267

Chang A, Foster J, Hall D (1987) Nimbus-7 SMMR derived global snow cover parameters. Ann Glaciol 9(9):39–44

Chang A, Foster J, Kelly R, Josberger E, Armstrong R, Mognard N (2005) Analysis of ground-measured and passive-microwave-derived snow depth variations in midwinter across the northern Great Plains. J Hydrometeorol 6(1):20–33

Clifford D (2010) Global estimates of snow water equivalent from passive microwave instruments: history, challenges and future developments. Int J Remote Sens 31(14):3707–3726

Colbeck S (1982) An overview of seasonal snow metamorphism. Rev Geophys 20(1):45–61

Colliander A, Chan S, Kim S-B, Das N, Yueh S, Cosh M, Bindlish R, Jackson T, Njoku E (2012) Long term analysis of PALS soil moisture campaign measurements for global soil moisture algorithm development. Remote Sens Environ 121:309–322. doi:10.1016/j.rse.2012.02.002

Cork H, Loijens H (1980) The effect of snow drifting on gamma snow survey results. J Hydrol 48 (1–2):41–51

Davenport I, Sandells M, Gurney R (2012) The effects of variation in snow properties on passive microwave snow mass estimation. Remote Sens Environ 118:168–175

Dietz AJ, Kuenzer C, Gessner U, Dech S (2012) Remote sensing of snow—a review of available methods. Int J Remote Sens 33(13):4094–4134

Dong J, Walker JP, Houser PR (2005) Factors affecting remotely sensed snow water equivalent uncertainty. Remote Sens Environ 97(1):68–82

Foster J, Rango A, Hall D, Chang A, Allison L, Diesen B (1980) Snowpack monitoring in North America and Eurasia using passive microwave satellite data. Remote Sens Environ 10 (4):285–298

Foster JL, Barton J, Chang AT, Hall DK (2001) Snow crystal and land cover effects on the scattering of passive microwave radiation for algorithm development. In: Europto Remote Sensing 2001. International Society for Optics and Photonics, pp 149–155

Frei A, Tedesco M, Lee S, Foster J, Hall DK, Kelly R, Robinson DA (2012) A review of global satellite-derived snow products. Adv Space Res 50(8):1007–1029

Gan TY, Kalinga O, Singh P (2009) Comparison of snow water equivalent retrieved from SSM/I passive microwave data using artificial neural network, projection pursuit and nonlinear regressions. Remote Sens Environ 113(5):919–927

Giddings JC, LaChapelle E (1962) The formation rate of depth hoar. J Geophys Res 67 (6):2377–2383

Grasty R (1982) Direct snow-water equivalent measurement by air-borne gamma-ray spectrometry. J Hydrol 55(1–4):213–235

Grenfell T, Putkonen J (2008) A method for the detection of the severe rain-on-snow event on Banks Island, October 2003, using passive microwave remote sensing. Water Resour Res 44 (3), W03425

Hall DK, Kelly REJ, Foster JL, Chang ATC (2006) Estimation of snow extent and snow properties. In: Encyclopedia of hydrological sciences. Wiley, New York

Hallikainen MT (1989) Microwave radiometry of snow. Adv Space Res 9(1):267–275

Hallikainen MT, Ulaby FT, Abdelrazik M (1986) Dielectric properties of snow in the 3 to 37 GHz range. IEEE Trans Antennas Propag 34(11):1329–1340

Hancock S, Baxter R, Evans J, Huntley B (2013) Evaluating global snow water equivalent products for testing land surface models. Remote Sens Environ 128:107–117

Harr RD (1981) Some characteristics and consequences of snowmelt during rainfall in western Oregon. J Hydrol 53(3):277–304. doi:10.1016/0022-1694(81)90006-8

Hirsch R, Ryberg K (2012) Has the magnitude of floods across the USA changed with global CO2 levels? Hydrol Sci J 57(1):1–9

Jackson TJ III (1993) Measuring surface soil moisture using passive microwave remote sensing. Hydrol Process 7(2):139–152

Jackson TJ, Cosh MH, Bindlish R, Starks PJ, Bosch DD, Seyfried M, Goodrich DC, Moran MS, Du J (2010) Validation of advanced microwave scanning radiometer soil moisture products. IEEE Trans Geosci Remote Sens 48(12):4256–4272

Jackson TJ, Bindlish R, Cosh MH, Zhao T, Starks PJ, Bosch DD, Seyfried M, Moran MS, Goodrich DC, Kerr YH, Leroux D (2012) Validation of soil moisture and ocean salinity (SMOS) soil moisture over watershed networks in the U.S. IEEE Trans Geosci Remote Sens 50(5):1530–1543. doi:10.1109/TGRS.2011.2168533

Jacobs JM, Myers DA, Whitfield BM (2003) Improved rainfall/runoff estimates using remotely sensed soil moisture. J Am Water Resour Assoc 39(2):313–324. doi:10.1111/j.1752-1688.2003.tb04386.x

Jones WK, Carroll TR (1983) Error analysis of airborne gamma radiation soil moisture measurements. Agric Meteorol 28(1):19–30

Jones LA, Kimball JS, Podest E, McDonald KC, Chan SK, Njoku EG (2009) A method for deriving land surface moisture, vegetation optical depth, and open water fraction from AMSR-E. In: Geoscience and Remote Sensing Symposium, 2009 I.E. International, IGARSS 2009. IEEE, pp III-916–III-919

Josberger EG, Mognard NM (2002) A passive microwave snow depth algorithm with a proxy for snow metamorphism. Hydrol Process 16(8):1557–1568

Josberger E, Mognard N, Lind B, Matthews R, Carroll T (1998) Snowpack water-equivalent estimates from satellite and aircraft remote-sensing measurements of the Red River Basin, north-central USA. Ann Glaciol 26:119–124

Kang DH, Barros AP, Dery SJ (2014) Evaluating passive microwave radiometry for the dynamical transition from dry to wet snowpacks. IEEE Trans Geosci Remote Sens 52(1):3–15

Kelly R (2009) The AMSR-E snow depth algorithm: description and initial results. J Remote Sens Soc Jpn 29(1):307–317

Kelly RE, Chang AT, Tsang L, Foster JL (2003) A prototype AMSR-E global snow area and snow depth algorithm. IEEE Trans Geosci Remote Sens 41(2):230–242

Kerr YH, Waldteufel P, Richaume P, Wigneron JP, Ferrazzoli P, Mahmoodi A, Al Bitar A, Cabot F, Gruhier C, Juglea SE (2012) The SMOS soil moisture retrieval algorithm. IEEE Trans Geosci Remote Sens 50(5):1384–1403

Knox JC (2000) Sensitivity of modern and Holocene floods to climate change. Quat Sci Rev 19 (1–5):439–457. doi:10.1016/S0277-3791(99)00074-8

Koster RD, Guo Z, Yang R, Dirmeyer PA, Mitchell K, Puma MJ (2009) On the nature of soil moisture in land surface models. J Climate 22(16):4322–4335

Kreller M, Plumb EW, Holloway E, Li S (2016) River ice and flood detection products derived from Suomi NPP VIIRS satellite data to support 2015 hydrologic forecast operations in Alaska. In: Paper presented at the American Meteorological Society Annual Meeting, New Orleans, LA, 10–14 Jan 2016

Leroux DJ, Das NN, Entekhabi D, Colliander A, Njoku E, Jackson TJ, Yueh S (2016) Active-passive soil moisture retrievals during the SMAP validation experiment 2012. IEEE Geosci Remote Sens Lett 13(4):475–479. doi:10.1109/LGRS.2015.2491643

Liu YY, Parinussa RM, Dorigo WA, De Jeu RAM, Wagner W, van Dijk AIJM, McCabe MF, Evans JP (2011) Developing an improved soil moisture dataset by blending passive and active microwave satellite-based retrievals. Hydrol Earth Syst Sci 15(2):425–436. doi:10.5194/hess-15-425-2011

Luojus K, Pulliainen J, Takala M, Lemmetyinen J, Kangwa M, Smolander T, Derksen C (2013) Global snow monitoring for climate research (GlobSnow) algorithm theoretical basis document—SWE-algorithm. p 35

Mätzler C (1987) Applications of the interaction of microwaves with the natural snow cover. Remote Sens Rev 2(2):259–387

Miller JE, Frink DL (1984) Changes in flood response of the Red River of the North basin, North Dakota-Minnesota. United States Government Printing Office, Washington, DC

Mognard M, Josberger EG (2002) Northern great plains 1996/97 seasonal evolution of snowpack parameters from satellite passive-microwave measurements. Ann Glaciol 34(1):15–23

Mote TL, Grundstein AJ, Leathers DJ, Robinson DA (2003) A comparison of modeled, remotely sensed, and measured snow water equivalent in the northern Great Plains. Water Resour Res 39 (8):1209

NALCMS (2015) 2010 North American Land Cover at 250 m spatial resolution. In: North American Land Change Monitoring System. Natural Resources Canada/Canadian Center for Remote Sensing (NRCan/CCRS), U.S.G.S.U., Instituto Nacional de Estadística y Geografía (INEGI), Comisión Nacional para el Conocimiento y Uso de la Biodiversidad (CONABIO), and Comisión Nacional Forestal (CONAFOR)

Njoku EG, Entekhabi D (1996) Passive microwave remote sensing of soil moisture. J Hydrol 184 (1–2):101–129. doi:10.1016/0022-1694(95)02970-2

Njoku EG, Jackson TJ, Lakshmi V, Chan TK, Nghiem SV (2003) Soil moisture retrieval from AMSR-E. IEEE Trans Geosci Remote Sens 41(2):215–229

NWS-HIC (2011) United States Flood Loss Report—Water Year 2011. In: NWS Annual Flood Loss Summary Reports to U.S. Army Corps of Engineers. NOAA National Weather Service-Hydrologic Information Center

Owe M, De Jeu R, Walker J (2001) A methodology for surface soil moisture and vegetation optical depth retrieval using the microwave polarization difference index. IEEE Trans Geosci Remote Sens 39(8):1643–1654

Peck EL, Bissell V, Jones E, Burge D (1971) Evaluation of snow water equivalent by airborne measurement of passive terrestrial gamma radiation. Water Resour Res 7(5):1151–1159

Peck EL, Carroll TR, VanDemark SC (1980) Operational aerial snow surveying in the United States/Etude de neige aérienne effectuée aux Etats Unis. Hydrol Sci J 25(1):51–62

Pulliainen J (2006) Mapping of snow water equivalent and snow depth in boreal and sub-arctic zones by assimilating space-borne microwave radiometer data and ground-based observations. Remote Sens Environ 101(2):257–269. doi:10.1016/j.rse.2006.01.002

Quiring SM, Ford TW, Wang JK, Khong A, Harris E, Lindgren T, Goldberg DW, Li Z (in press) The North American Soil Moisture Database: Development and Applications. Bulletin of the American Meteorological Society 97(8). doi:10.1175/BAMS-D-13-00263.1

Rahman MM, Lin Z, Jia X, Steele DD, DeSutter TM (2014) Impact of subsurface drainage on streamflows in the Red River of the North basin. J Hydrol 511:474–483

Ramage JM, Isacks BL (2002) Determination of melt-onset and refreeze timing on southeast Alaskan icefields using SSM/I diurnal amplitude variations. Ann Glaciol 34(1):391–398

Rango A II (1993) Snow hydrology processes and remote sensing. Hydrol Process 7(2):121–138

Rannie W (2016) The 1997 flood event in the Red River basin: causes, assessment and damages. Can Water Resour J 41(1–2):45–55. doi:10.1080/07011784.2015.1004198

Rasmussen PF (2016) Assessing the impact of climate change on the frequency of floods in the Red River Basin. Can Water Resour J 41(1–2):331–342. doi:10.1080/07011784.2015.1025101

Reichle RH (2008) Data assimilation methods in the Earth sciences. Adv Water Resour 31 (11):1411–1418

Reichle RH, Koster RD (2004) Bias reduction in short records of satellite soil moisture. Geophys Res Lett 31(19):L19501

Rijal S, Zhang X, Jia X (2013) Estimating surface soil water content in the Red River Valley of the North using Landsat 5 TM data. Soil Sci Soc Am J 77(4):1133–1143

Rogers P, Kaiser J, Kellenbenz D, Ewens M (2013) A comparative hydrometeorological analysis of the 2009, 2010, and 2011 Red River of the North Basin Spring floods. National Weather Service, Central Region Technical Attachment Number 13-03

Santi E, Pettinato S, Paloscia S, Pampaloni P, Macelloni G, Brogioni M (2012) An algorithm for generating soil moisture and snow depth maps from microwave spaceborne radiometers: HydroAlgo. Hydrol Earth Syst Sci 16(10):3659–3676

Schaefer GL, Cosh MH, Jackson TJ (2007) The USDA natural resources conservation service soil climate analysis network (SCAN). J Atmos Oceanic Tech 24(12):2073–2077

Schwert DP (2003) A geologist's perspective on the Red River of the North: history, geography, and planning/management issues. In: Proceedings of 1st International Water Conference, Red River Basin Institute, Moorhead, MN

Shanley JB, Chalmers A (1999) The effect of frozen soil on snowmelt runoff at Sleepers River, Vermont. Hydrol Process 13(12–13):1843–1857. doi:10.1002/(SICI)1099-1085(199909)13:12/13<1843::AID-HYP879>3.0.CO;2-G

Singh PR, Gan TY (2000) Retrieval of snow water equivalent using passive microwave brightness temperature data. Remote Sens Environ 74(2):275–286

Stadnyk T, Dow K, Wazney L, Blais E-L (2016) The 2011 flood event in the Red River Basin: causes, assessment and damages. Can Water Resour J 41(1–2):65–73. doi:10.1080/07011784.2015.1008048

Sturm M, Holmgren J, Liston GE (1995) A seasonal snow cover classification system for local to global applications. J Climate 8(5):1261–1283

Sturm M, Taras B, Liston GE, Derksen C, Jonas T, Lea J (2010) Estimating snow water equivalent using snow depth data and climate classes. J Hydrometeorol 11(6):1380–1394

Takala M, Luojus K, Pulliainen J, Derksen C, Lemmetyinen J, Kärnä J-P, Koskinen J, Bojkov B (2011) Estimating northern hemisphere snow water equivalent for climate research through

assimilation of space-borne radiometer data and ground-based measurements. Remote Sens Environ 115(12):3517–3529
Tedesco M, Narvekar PS (2010) Assessment of the NASA AMSR-E SWE Product. IEEE J Sel Top Appl Earth Observ Remote Sens 3(1):141–159
Tedesco M, Pulliainen J, Takala M, Hallikainen M, Pampaloni P (2004) Artificial neural network-based techniques for the retrieval of SWE and snow depth from SSM/I data. Remote Sens Environ 90(1):76–85
Todhunter PE (2001) A hydroclimatological analysis of the Red River of the North Snowmelt Flood Catastrophe of 1997. J Am Water Resour Assoc 37:1263–1278
Ulaby FT, Stiles WH (1980) The active and passive microwave response to snow parameters: 2. Water equivalent of dry snow. J Geophys Res Oceans 85(C2):1045–1049. doi:10.1029/JC085iC02p01045
Ulaby FT, Moore RK, Fung AK (1981) Microwave remote sensing: active and passive. Microwave remote sensing, fundamentals and radiometry, vol 1. Addison-Wesley, Reading, MA
Vuyovich C, Jacobs JM (2011) Snowpack and runoff generation using AMSR-E passive microwave observations in the Upper Helmand Watershed, Afghanistan. Remote Sens Environ 115 (12):3313–3321
Vuyovich CM, Jacobs JM, Daly SF (2014) Comparison of passive microwave and modeled estimates of total watershed SWE in the continental United States. Water Resour Res 50 (11):9088–9102
Wagner W, Hahn S, Kidd R, Melzer T, Bartalis Z, Hasenauer S, Figa-Saldaña J, de Rosnay P, Jann A, Schneider S (2013) The ASCAT soil moisture product: a review of its specifications, validation results, and emerging applications. Meteorol Z 22(1):5–33
Walker A, Goodison B (1993) Discrimination of a wet snowcover using passive microwave satellite data. Ann Glaciol 17:307–311
Wang JR, Tedesco M (2007) Identification of atmospheric influences on the estimation of snow water equivalent from AMSR-E measurements. Remote Sens Environ 111(2–3):398–408. doi:10.1016/j.rse.2006.10.024
Wang Y, Colby J, Mulcahy K (2002) An efficient method for mapping flood extent in a coastal floodplain using Landsat TM and DEM data. Int J Remote Sens 23(18):3681–3696
Wazney L, Clark SP (2016) The 2009 flood event in the Red River Basin: causes, assessment and damages. Can Water Resour J 41(1–2):56–64. doi:10.1080/07011784.2015.1009949
Wilson BA, Rashid H (2005) Monitoring the 1997 flood in the Red River Valley using hydrologic regimes and RADARSAT imagery. Can Geogr 49(1):100–109
Winther JG, Hall DK (1999) Satellite-derived snow coverage related to hydropower production in Norway: present and future. Int J Remote Sens 20(15–16):2991–3008. doi:10.1080/014311699211570
WMO (2009) WMO-No. 168. Guide to hydrometeorological practices. World Meteorological Organization, Geneva, Switzerland
Zhan X, Sohlberg R, Townshend J, DiMiceli C, Carroll M, Eastman J, Hansen M, DeFries R (2002) Detection of land cover changes using MODIS 250 m data. Remote Sens Environ 83 (1):336–350

http://www.springer.com/978-3-319-43743-9

Remote Sensing of Hydrological Extremes
Lakshmi, V. (Ed.)
2017, XIV, 251 p. 74 illus., 71 illus. in color., Hardcover
ISBN: 978-3-319-43743-9